

ALMA Single Dish and Array Combination Workshop, 2012 Dec 17-19  
Heterogeneous Array Imaging

Melvyn Wright  
Radio Astronomy Laboratory, University of California, Berkeley, CA 94720

December 17, 2012

# Contents

<b>1</b>	<b>SUMMARY</b>	<b>4</b>
<b>2</b>	<b>ASTRONOMICAL REQUIREMENTS</b>	<b>6</b>
<b>3</b>	<b>LARGE FIELD IMAGING</b>	<b>7</b>
3.1	SHORT SPACING PROBLEM . . . . .	8
3.2	SAMPLING SHORT SPACINGS . . . . .	9
3.3	SINGLE DISH OBSERVATIONS . . . . .	11
<b>4</b>	<b>COMBINING SINGLE DISH AND INTERFEROMETER OBSERVATIONS</b>	<b>12</b>
4.1	EKERS AND ROTS . . . . .	16
4.2	COMBINING ALMA, ACA AND SINGLE DISH DATA . . . . .	18
<b>5</b>	<b>HETEROGENEOUS ARRAYS</b>	<b>19</b>
<b>6</b>	<b>POINTING AND PRIMARY BEAM CALIBRATION</b>	<b>21</b>
<b>7</b>	<b>MOSAICING ALGORITHMS</b>	<b>26</b>
7.1	MAPPING LARGE FIELD OF VIEW . . . . .	26
7.2	IMAGING LARGE SCALE STRUCTURE . . . . .	28
<b>8</b>	<b>LINEAR MOSAICING ALGORITHMS</b>	<b>29</b>
<b>9</b>	<b>MAXIMUM ENTROPY DECONVOLUTION</b>	<b>32</b>
<b>10</b>	<b>SAMPLING REQUIREMENT</b>	<b>38</b>

10.1 HEXAGONAL POINTING GRIDS . . . . .	39
<b>11 IMAGE FIDELITY AS A FUNCTION OF SOURCE SIZE</b>	<b>43</b>
<b>12 PRIMARY BEAMS IN MOSAICS</b>	<b>46</b>
<b>13 DECONVOLVING PRIMARY BEAM PATTERNS FROM MOSAICS</b>	<b>47</b>
<b>14 CONCLUSION</b>	<b>48</b>

## 1 SUMMARY

Aperture synthesis arrays sample the cross correlation of the signals from an array of antennas, or phased array stations in the case of the SKA. The signal from each antenna measures the sky brightness distribution weighted by the primary beam pattern.

Images of the sky brightness are formed by combining the measured cross correlations between the antenna stations. The usual assumption for aperture synthesis imaging is that the illumination of the sky by the primary beam pattern is invariant, and the same for all antenna stations. In this case an image of the primary beam weighted sky brightness can be formed from a Fourier transform of the measured cross correlations. Sources larger than the primary beam require a mosaic of interferometer and single dish observations at multiple pointing centers.

For a point source at the pointing center, e.g. a quasar calibration observation, the array response is well described by the forward gain. For an extended source distribution, the array response depends on the primary

beam illumination of the sky at each antenna.

The effects of amplitude and phase errors in the calibration of the measured cross correlations are well known. Less well appreciated are the effects of amplitude and phase errors in the primary beam illumination of an extended source distribution. The case for a homogeneous array of antennas has been well studied. The image fidelity for mosaic observations is severely limited by pointing and primary beam errors (Cornwell, Holdaway & Uson, 1993; Holdaway, 1998).

In this paper we review the requirements for mosaic observations with heterogeneous arrays of antennas and single dish telescopes. We discuss the errors from pointing and primary beam voltage patterns. These results are relevant to all aperture synthesis arrays, including millimeter/submillimeter wavelength arrays like ALMA, and cm/m wavelength arrays like ATA and SKA.

## 2 ASTRONOMICAL REQUIREMENTS

- Millimeter wavelength Imaging from Comets to Cosmology
  - Hale Bopp 1 AU 3 arcmin 0.1 arcsec (75 km)
  - Orion Core 500 pc 40 arcsec 0.1 arcsec (50 AU)
  - Cas A 3 kpc 5 arcmin 1 arcsec (3000 AU)
  - IC342 nucleus 2 Mpc 1 arcmin 1 arcsec (10 pc)
  - Cygnus A 200 Mpc 3 arcmin 1 arcsec (1 kpc)
  - Cluster Core 2 Gpc 3 arcmin 10 arcsec (100 kpc)
- Field of View several arcmin
- Resolution  $< \sim 0.1$  arcsec.
- Spatial dynamic range  $> \sim 1000$ .

### 3 LARGE FIELD IMAGING

- Arrays are good at mapping compact structures.
- Single dishes are good at mapping large scale structure.
- Telescopes are matched filters to a set of spatial scales.
- Importance for getting correct answers for spectral index, etc;
- Many astrophysical quantities are derived from ratios

$$^{13}\text{CO}/^{12}\text{CO} = I(^{13}\text{CO}) \star B(^{13}\text{CO}) / I(^{12}\text{CO}) \star B(^{12}\text{CO})$$

$$SI = \log[I(\nu_1) \star B(\nu_1)] - \log[I(\nu_2) \star B(\nu_2)] / [\log(\nu_1) - \log(\nu_2)]$$

WRONG answer, since  $a/b$  is not equal to  $(a - a')/(b - b')$

$a'$  and  $b'$  are unsampled large scale structure.

### 3.1 SHORT SPACING PROBLEM

- Interferometer array samples spacings from  $D_{min}$  to  $D_{max}$ .  
Source structure with angular scale  $> \lambda/2D_{min}$  is not sampled.  
Shortest spacing  $>$  dish diameter, else collision or shadowing.
- Negative sidelobes due to extended structure
- Shortest spacings are partially sampled.  
uv-samples in annulus between uv-min and uv-max  
synthesized beam  $\sim J_1(x)/x$  for uv-max, minus  $J_1(x)/x$  for uv-min.  
this causes a negative basin around the source.
- shortest spacings are often just a few Fourier components  
i.e. a few sine waves, with high amplitudes.  
Images may look better without them.  
convolve the uv-plane to make a smooth inner edge.

## 3.2 SAMPLING SHORT SPACINGS

- Single dish observations

Single dish samples spacings from 0 to  $D_{ant}$ .

interferometer array samples spacings from  $D_{min}$  to  $D_{max}$ .

ideal single dish  $D_{ant} \sim 2 \times D_{min}$ ; overlap for calibration.

- Multiple beams for each antenna

illumination pattern rotates on sky for Alt-Az antennas.

cross-talk between beams gives variable DC offsets.

- Heterogeneous antenna arrays.

CARMA 10.4, 6.1 and 3.5m antennas.

MMA proposal was for 4m and 10m antennas.

ALMA has 7m and 12m antennas.

- Mosaicing

Ekers and Rots 1979, Groningen IAU

Tim Cornwell non-linear mosaicing using MEM  
Bob Sault linear mosaic algorithm.  
MOSSDI and MOSMEM deconvolution.

### 3.3 SINGLE DISH OBSERVATIONS

- Single dish beam  $A(x, y)$  convolves the sky brightness  $I(x, y)$

$$I'(x, y) = I(x, y) \star A(x, y) \times \Pi(x, y)$$

- Fourier transform gives the visibility data sampled in the uv-plane

$$V'(u, v) = V(u, v) \times a(u, v) \star \pi(u, v)$$

$a(u, v)$  is the weighting of spatial frequencies sampled by single dish. sampled visibilities are convolved by  $\pi$ , the Fourier transform of  $\Pi$ .

uv-data are aliased if  $\pi < 2D_{ant}/\lambda$

sample single dish observations with  $\Pi < \lambda/2D_{ant}$  to avoid aliasing.

- Deconvolve SD observations to obtain short uv-spacings using  $a(u, v)$
- Holography directly measures  $a(u, v)$

Gaussian beam approximation may introduce significant errors

## 4 COMBINING SINGLE DISH AND INTERFEROMETER OBSERVATIONS

- Single dishes sample spacings from 0 to  $D_{ant}$ .  
zero spacing gives the total flux in the image
- Interferometer arrays sample spacings from  $D_{min}$  to  $D_{max}$ .
- Need overlap for cross calibration.  
ideal single dish  $D_{ant} \sim 2 \times D_{min}$   
ACA overlaps with single dish; ALMA overlaps with ACA
- IMMERGE linearly merges low and high resolution images.  
e.g. single dish and interferometer images:  
deconvolve single dish observations. uses FT of single dish beam.  
multiply by interferometer image primary beam patterns.  
cross calibrate using overlapping uv-data in an annulus.  
merge the two images together
- MOSAIC multiple pointings of array and single dish images.

INVERT options=mosaic, makes image from multiple pointings  
MOSMEM – deconvolve multiple pointings with total flux constraint.  
– deconvolve using the single dish image as a default image.  
– joint deconvolution of multiple pointings and single dish images.  
MOSSDI –clean deconvolution of multiple pointings

I ACA\_9\_01.-30.cas.0.05.uv1 230.0000 GHz

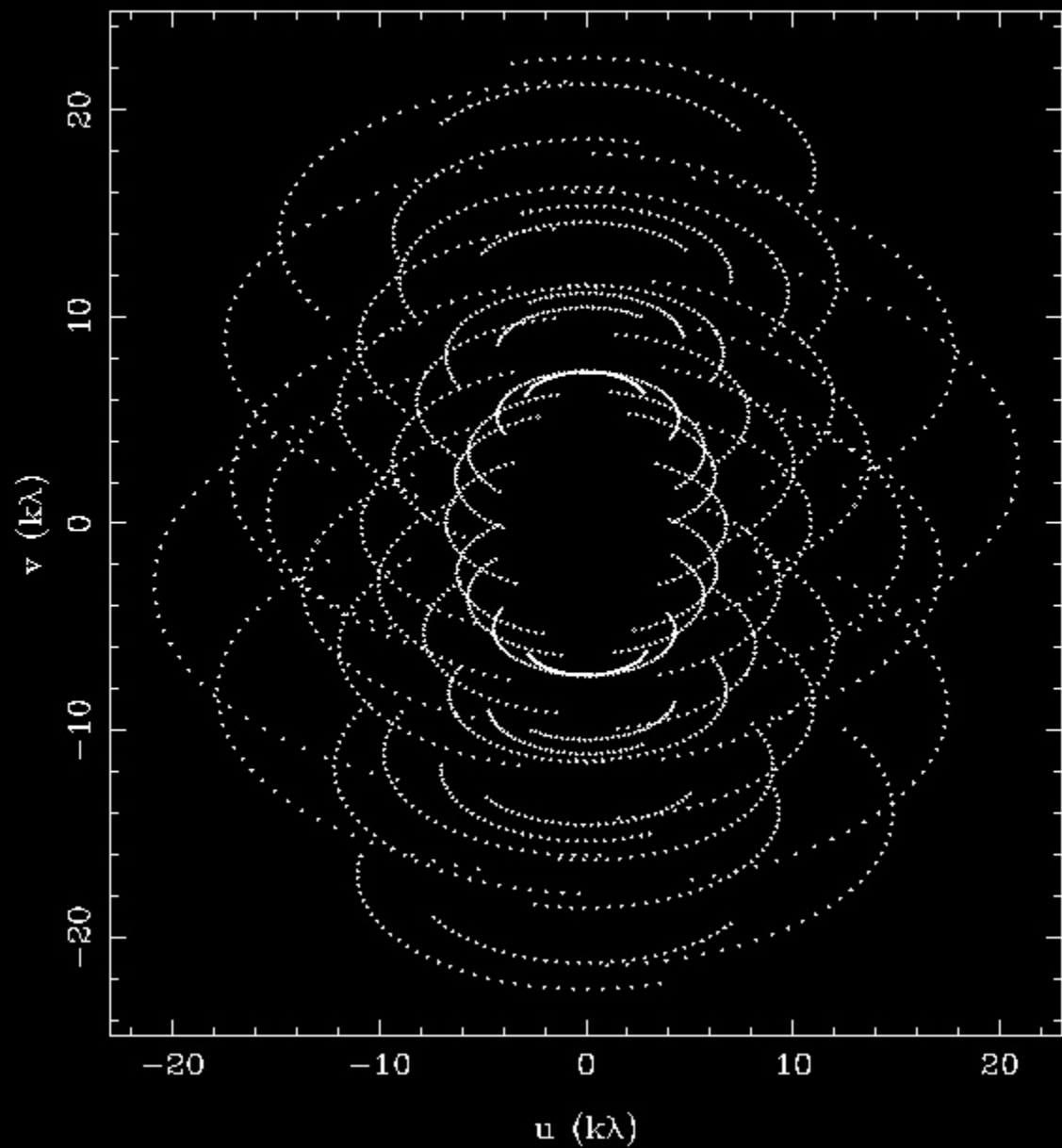


Figure 1: uv-sampling for ALMA Compact configuration ACA-9-01 at 230 GHz, HA +/- 4 h, DEC -30 .

I C32-3,-30.cas.0.05.uv1 230.0000 GHz

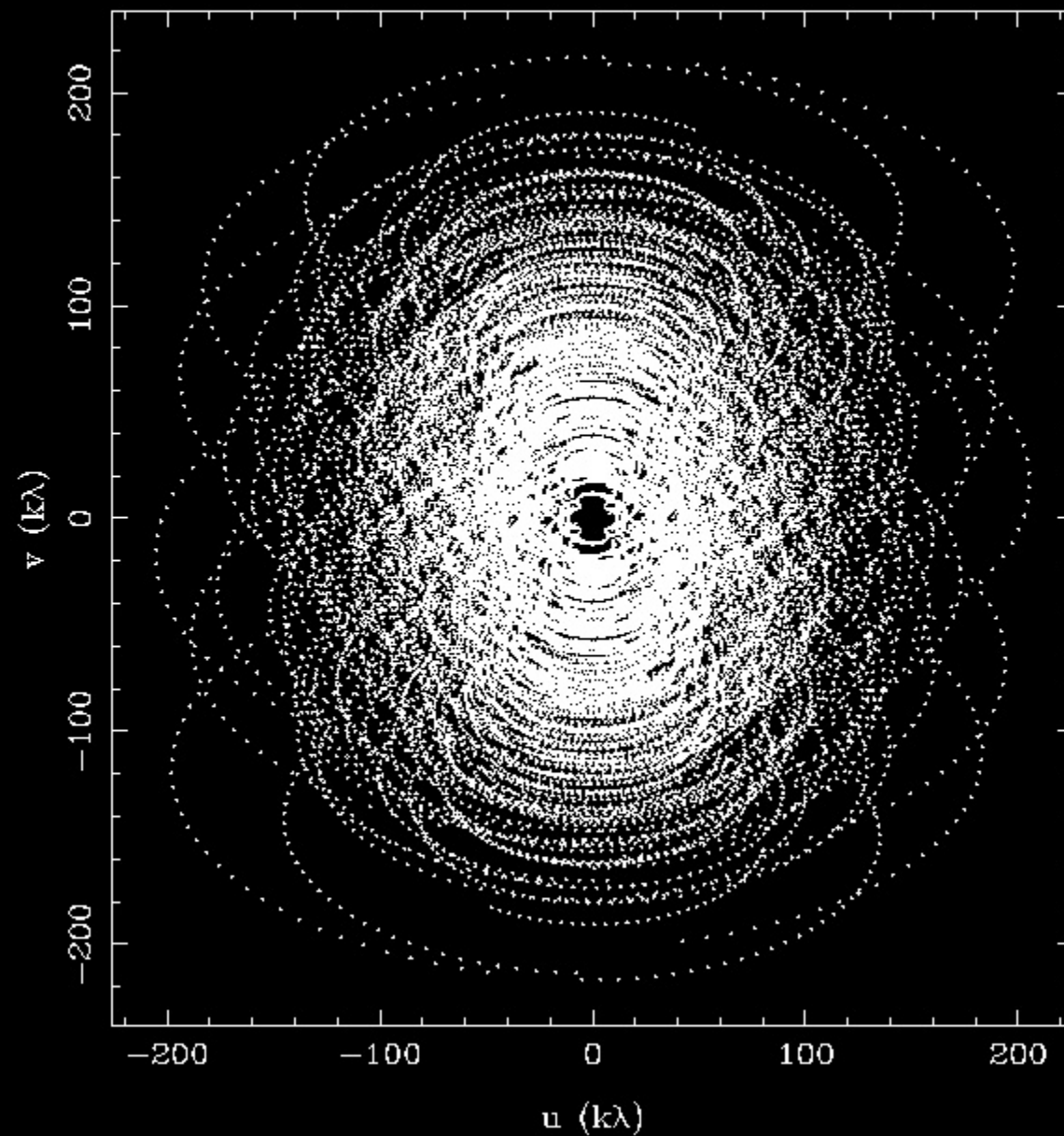


Figure 2: uv-sampling for ALMA cycle1 configuration C32-3 at 230 GHz, HA +/- 4 h, DEC -30 .

## 4.1 EKERS AND ROTS

- Mosaic observations sample visibilities around each  $(u,v)$  point.  
the wavefront is sampled across the antenna diameter,  $D_{ant}$ .

- Observations measure visibility at pointing center  $s'$

$$V(u, s') = \int I(s)A(s - s') \exp \frac{2\pi i}{\lambda} u s ds$$

- Phase gradients across aperture correlates different spacings.
- Observing a grid of pointings measures different Fourier samples.
- Fourier transform w.r.t. pointing measures visibilities around each  $(u,v)$  point.

$$V(u, u') = a(u') \times \int I(s)A(s - s') \exp \frac{2\pi i}{\lambda} (u + u') s ds$$

$$V(u, u') = a(u') \times V(u + u')$$

- In practice we recover  $\sim D_{ant}/2\lambda$  around each  $(u,v)$  sample.  
i.e. uv-tracks are  $\sim D_{ant}/\lambda$  wide, multiplied by  $a(u')$
- Need single dish observations to sample  $< D_{ant}/\lambda$  with good SNR.
- UVPNT uses Ekers and Rots algorithm to make uv-data from multiple pointings.

## 4.2 COMBINING ALMA, ACA AND SINGLE DISH DATA

- Best method depend strongly on calibration and systematic errors.
- Simulations assume 1'' RMS for both ACA and ALMA, and 1 percent gain stability for SDs.
- MIRIAD can combine ALMA + ACA + SD in one step.
- More secure approach is to cross calibrate and combine in steps. e.g.
  - ACA+SD enhanced low resolution image to combine with ALMA.
  - ALMA+SD with the common 12m PB, then add in ACA.
  - ALMA+ACA image, then joint deconvolution with SD.
- Compare the FT of the SD with ACA uv-data in overlap region.
  - use ACA to correct SD data and improve low resolution image.
  - remove systematic errors. e.g. PB astigmatism.
- Compare ACA and ALMA uv-data using image model and PB models.
  - make consistent calibration between SD, ACA and ALMA data.

## 5 HETEROGENEOUS ARRAYS

- Extended sources need correcting for the primary beam patterns.
- Sky is illuminated by PB voltage patterns for each pair of antennas.  
for each antenna pair  $(i, j)$ ,

$$P_{i,j}(\mathbf{s}) = V_i(\mathbf{s}) \times V_j^*(\mathbf{s})$$

primary beam patterns depend on the aperture illumination.

- PBs from 7 x 7, 12 x 12, and 7 x 12m cross-correlations.  
7 x 12m enhances SNR of 7m calibrations. (ALMA memo 272)
- All images are mosaics – even with only 1 pointing center.
- Mosaicing algorithms clip primary beam at  $\sim 5\%$  level,  
avoids uncertainties in primary beam at low levels.  
within 5%, PB pattern  $\sim$  Gaussian.  
outside 5%, there may be significant PB errors.

- What are typical measured PB errors ?

Pointing and PB errors at 100 and at 650 GHz ?

Are some antennas better or worse ?

What are differences in PB between 3 types of 12m antennas ?

## 6 POINTING AND PRIMARY BEAM CALIBRATION

- Primary beam is the product of voltage patterns for each antenna pair.
- PB is complex valued if pointing and voltage patterns are not identical.  
amplitude and phase errors in the visibility data hard to determine.
- Use same pointing pattern for all antennas  
reduces number of PB types and minimizes PB errors.  
if pointing centers are offset, asymmetric PB patterns rotate on sky.
- Pointing and Primary beam errors degrade the image fidelity.
- We should calculate a PB for each pointing, baseline, and integration.  
possible in principal, but the computing burden is substantial.
- Simulations use common mode and random pointing with  $\text{RMS} \sim 1''$   
Image fidelity reduced from 650 to 408 in a 19-pointing mosaic.  
Image errors depend on the time constant of the pointing errors.  
Overlap reduces weight of pointing errors and PB errors in a mosaic.

- Image point sources at different points in the PB pattern.  
how does the image fidelity varies across the primary beam ?

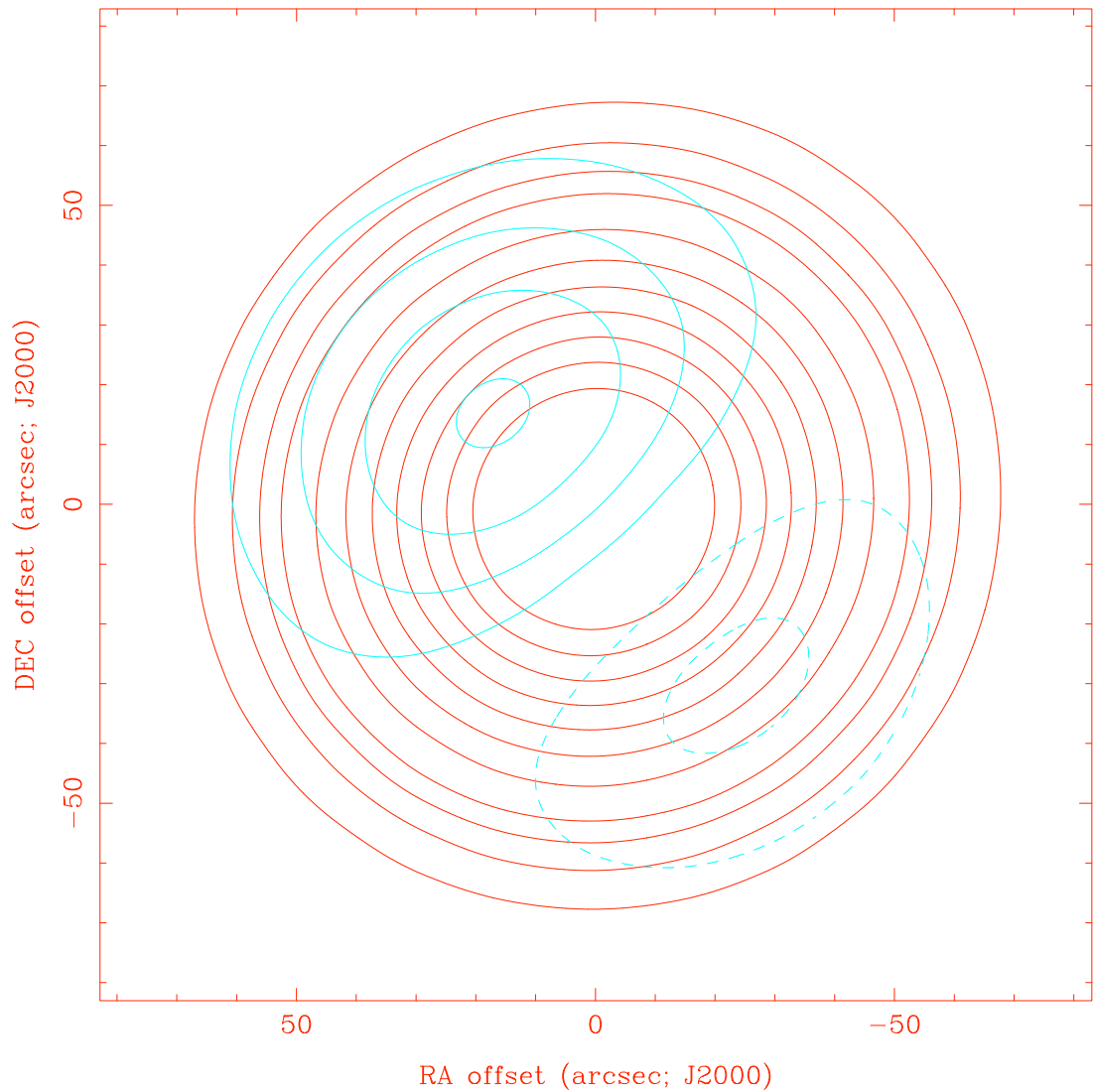


Figure 3: Complex Primary beam between antennas with offset illumination. The red contours are the real part of the primary beam response. The blue contours are the imaginary part of the primary beam response. contour levels= $-.2, -.15, -.1, -.05, .05, .10, .15, .2, .3, .4, .5, .6, .7, .8, .9$

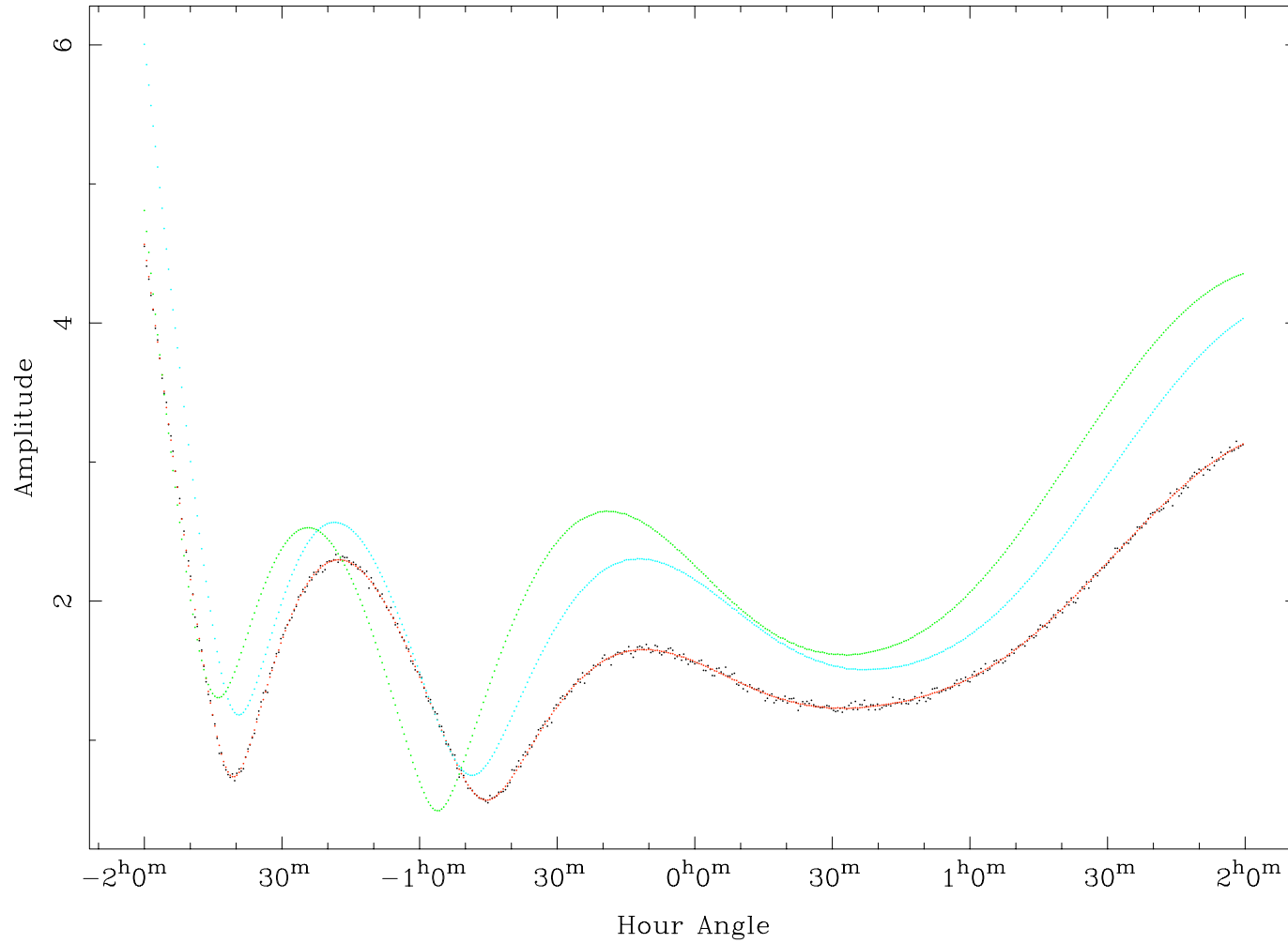


Figure 4: Amplitude errors in uv-data from two antennas offset illumination. Black points are the simulated uv-data. The red curve is the model visibility for the Gaussian model primary beam pattern used to generate the uv-data. blue curve is the model visibility using only real part of measured primary beam. green curve is the model visibility using the real and imaginary parts of the measured primary beam.

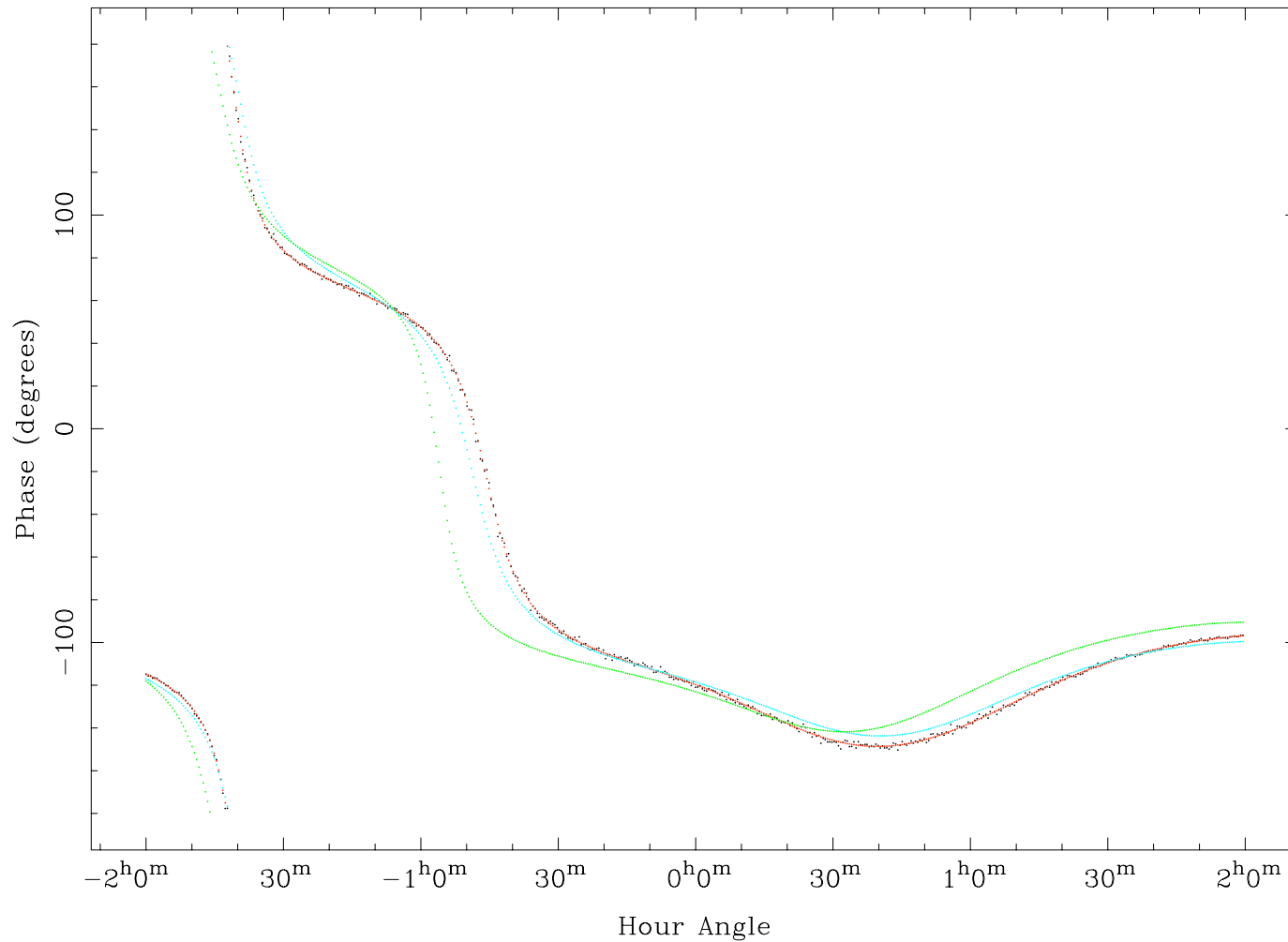


Figure 5: Phase errors in uv-data from two antennas offset illumination. Black points are the simulated uv-data. The red curve is the model visibility for the Gaussian model primary beam pattern used to generate the uv-data. blue curve is the model visibility using only real part of measured primary beam. green curve is the model visibility using the real and imaginary parts of the measured primary beam.

## 7 MOSAICING ALGORITHMS

- Two problems:
  1. Mapping a large field of view.
  2. Imaging large scale structure.

### 7.1 MAPPING LARGE FIELD OF VIEW

- Same as single dish mapping
- Scan antennas across the source and sample sky at Nyquist
- Primary beams  $A(x, y)$  convolve the sky brightness distribution  $I(x, y)$  sampled at intervals  $\delta\theta$  by  $\Pi$

$$I'(x, y) = I(x, y) \star A(x, y) \times \Pi(x, y)$$

- Fourier transform gives the visibility data sampled in the uv-plane

$$V'(u, v) = V(u, v) \times a(u, v) \star \pi(u, v)$$

$a(u, v)$  is the weighting of spatial frequencies sampled by PB.  
sampled visibilities are convolved by  $\pi$ , the Fourier transform of  $\Pi$ .  
uv-data are aliased if  $\pi < 2D_{ant}/\lambda$   
sample pointings with  $\delta\theta < \lambda/2D_{ant}$  to avoid aliasing uv-data.

## 7.2 IMAGING LARGE SCALE STRUCTURE

- Interferometer image  $I'(x, y)$

$$I'(x, y) = \int W(u, v)V(u, v) \exp \frac{-2\pi i}{\lambda}(ux + vy) dudv$$

$$I'(x, y) = I(x, y) \times A(x, y) \star B(x, y)$$

- Fourier plane measured visibility  $V'(u, v)$  is:

$$V'(u, v) = V(u, v) \star a(u, v) \times W(u, v)$$

$W(u, v)$  is the sampling in the uv-plane.

$a(u, v)$  is the weighting of spatial frequencies sampled by PB.

image is convolved by  $B(x, y)$ .

image is aliased if  $\delta uv > D_{ant}/2\lambda$ .

sample uv-data  $\delta uv < D_{ant}/2\lambda$  to avoid aliasing in sky plane.

## 8 LINEAR MOSAICING ALGORITHMS

- Primary beam weighted linear combination of pointings.

$$I'(x) = g(x) \Sigma (A(x - x_i) I_i(x) / \sigma_i^2) / (\Sigma A^2(x - x_i) / \sigma_i^2)$$

- MIRIAD **invert options=mosaic** – just like single field imaging.
- $g(x)$  is residual primary beam pattern to keep noise constant across mosaic image
- Synthesized beam is different for each pointing.  
synthesized beam has  $Npts$  image planes.
- Sidelobes  $\sim 1/Npts$
- Pointing errors may be common to adjacent pointings
- Gain and phase errors may be common to adjacent pointings
- Observing strategy is to sample all pointings in short time interval.
- Selfcal can be used with multiple pointing centers.

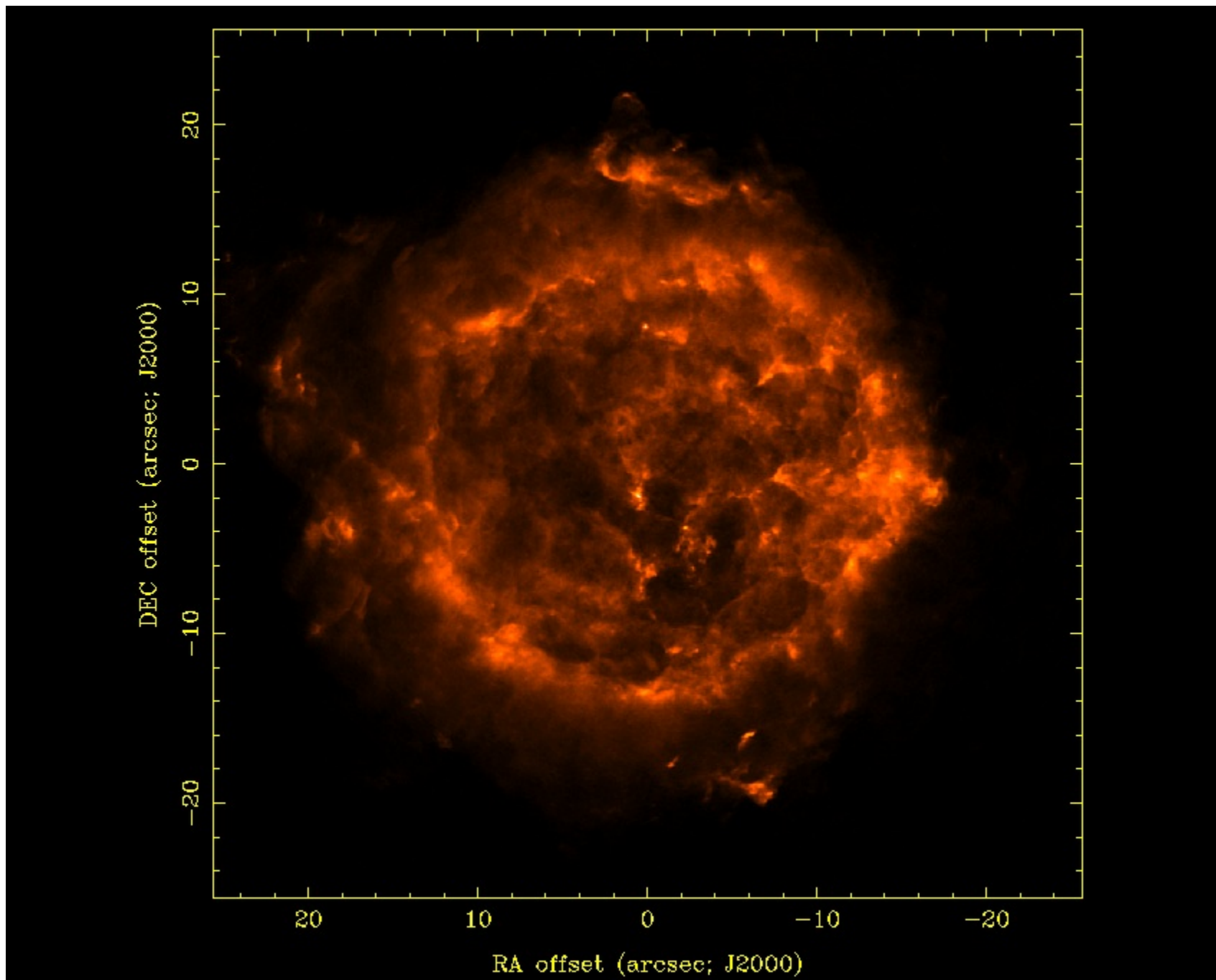


Figure 6: Image model is scaled VLA image of Cas A supernova remnant. Fractal structures on all scales.

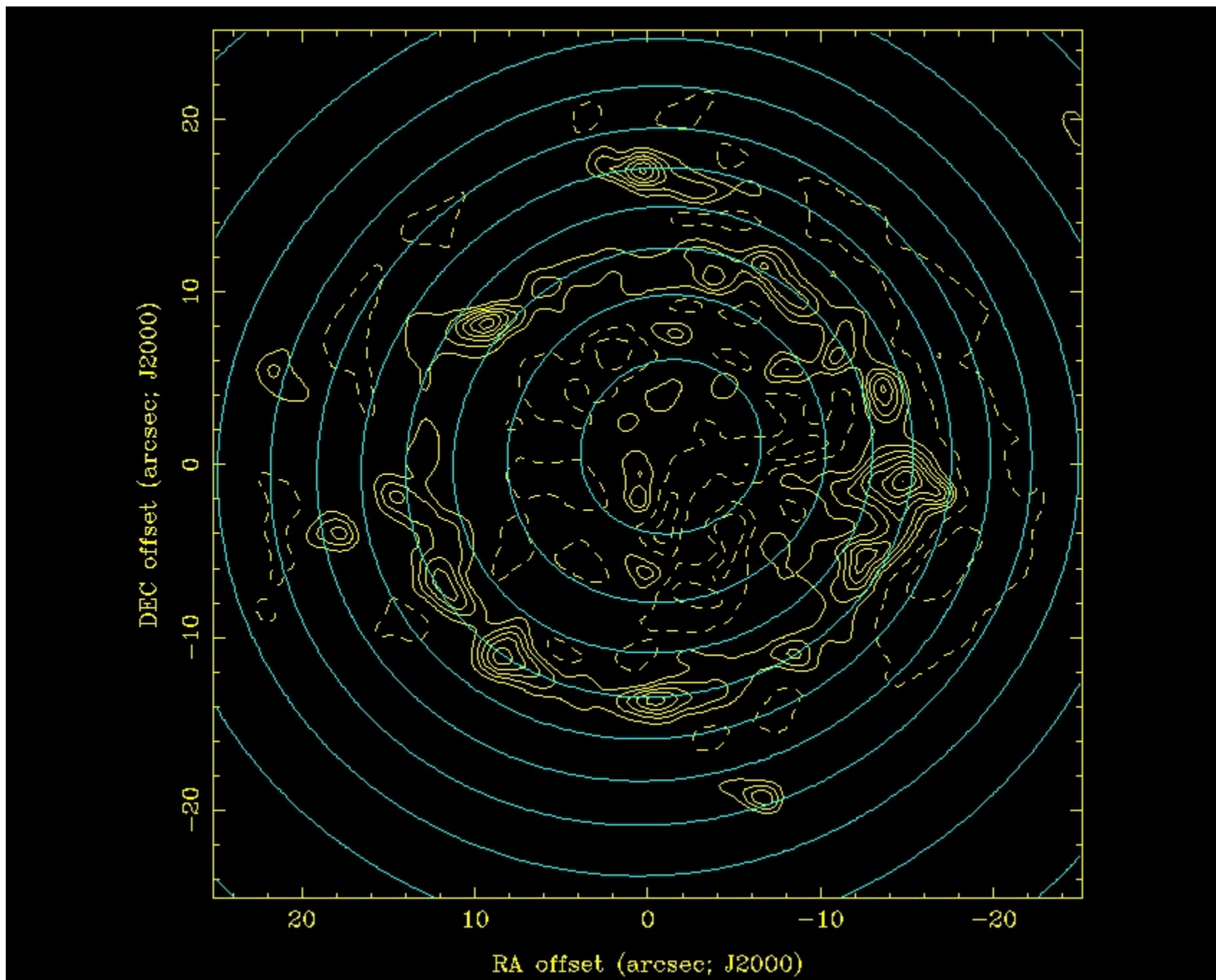


Figure 7: 19-pointing mosaic and single dish image for ALMA cycle1 configuration C32-3 at 230 GHz, HA +/- 4 h, DEC -30 .

## 9 MAXIMUM ENTROPY DECONVOLUTION

- Maximize entropy,  $H$ , consistent with observations:

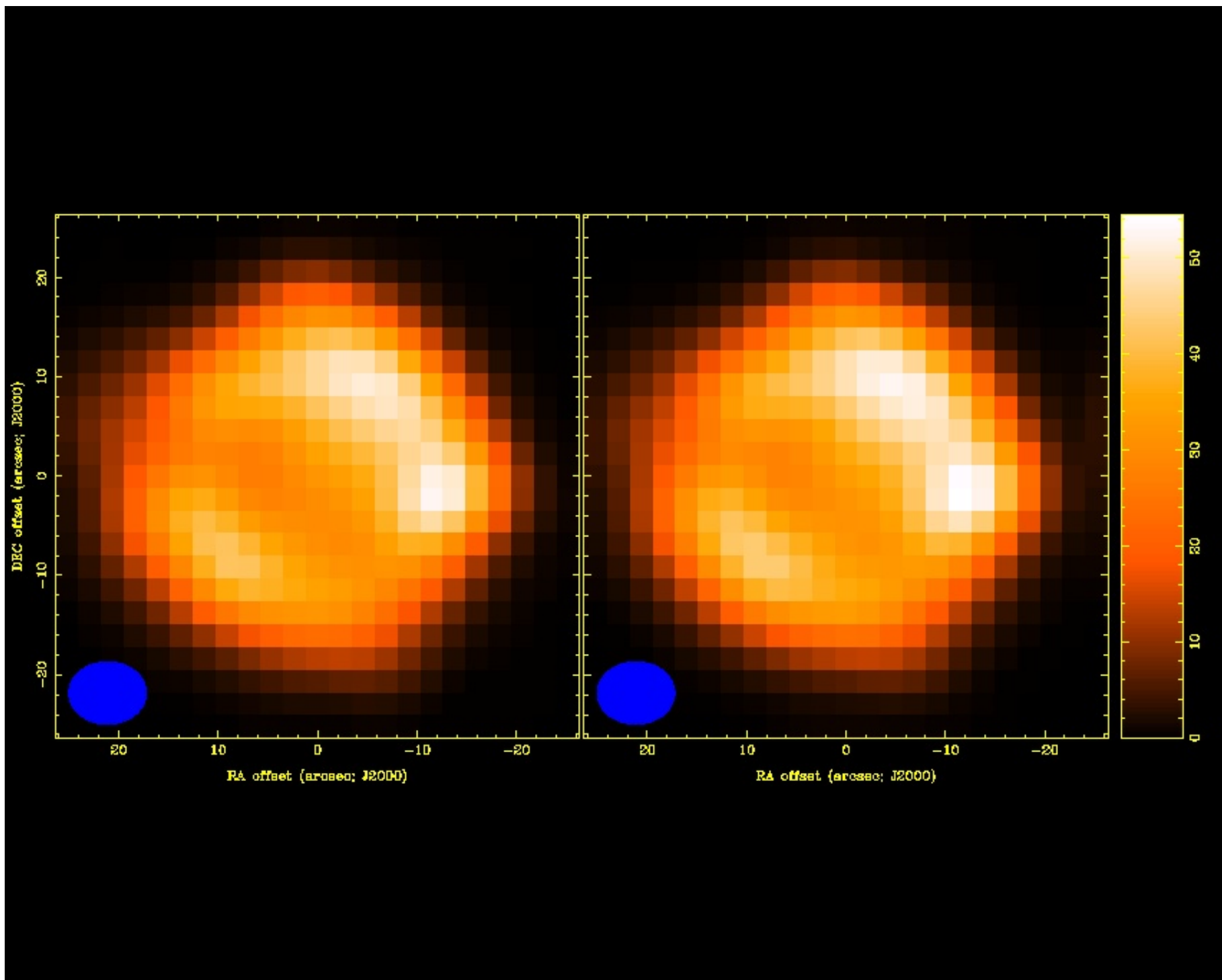
$$H = -\sum I \log(I/M e)$$

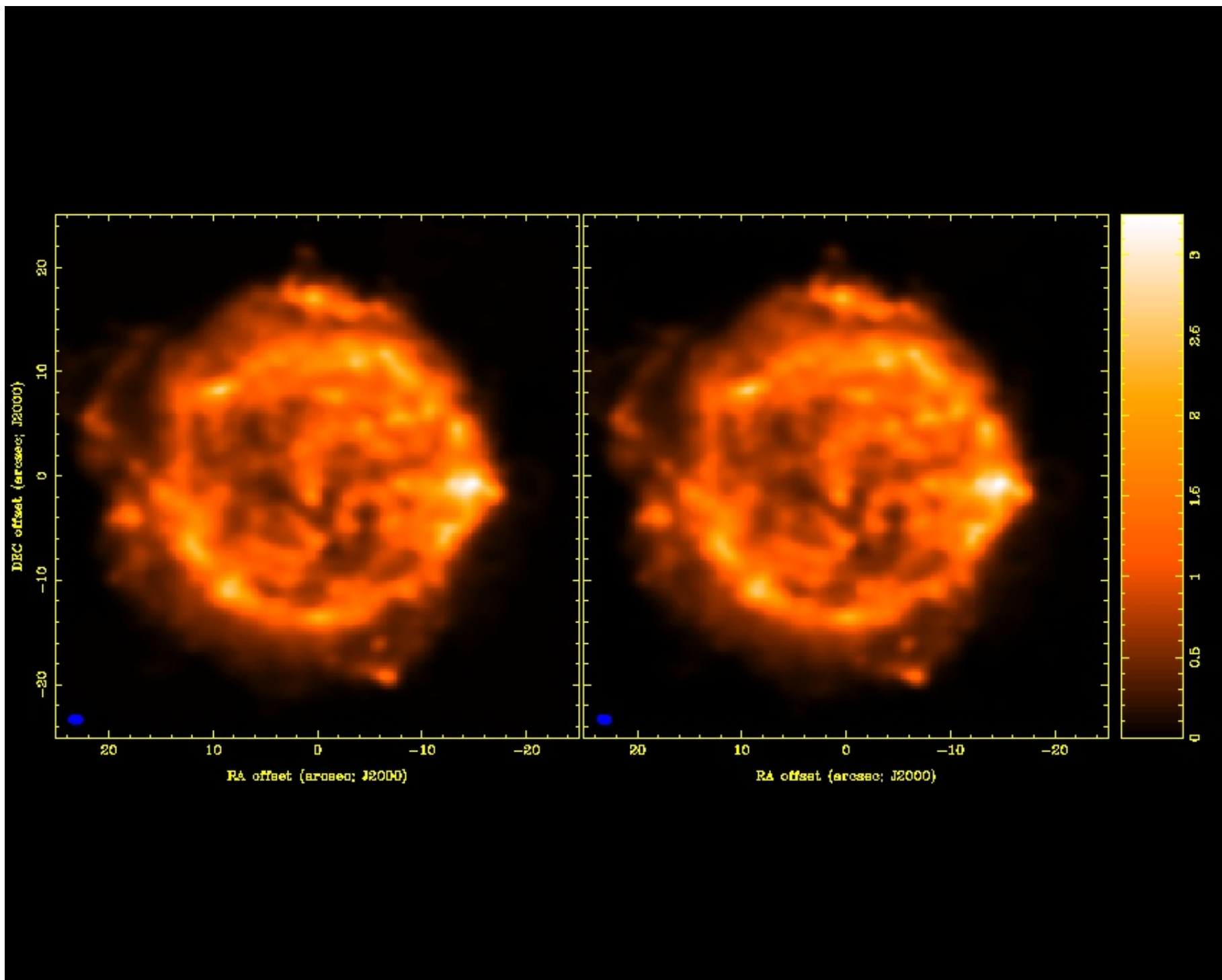
subject to  $\chi^2$  constraint summed over all pointings  $(x', y')$

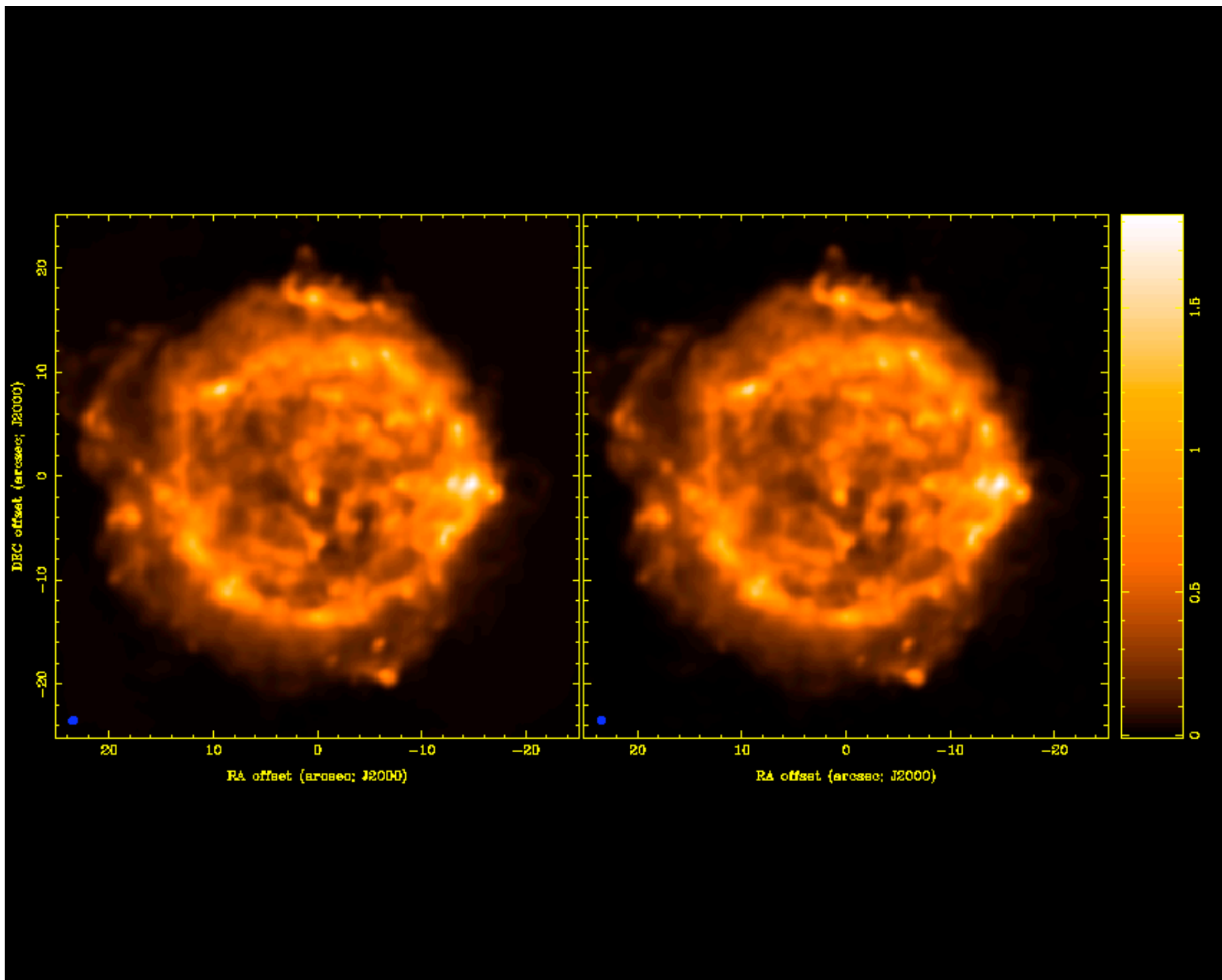
$$\chi^2 = \sum (V'(u, v, x', y') - V(u, v, x', y'))^2 / \sigma(u, v, x', y')^2$$

- Entropy measure: either "gull" ( $-p \log(p/e)$ ) or "cornwell" ( $-\log(\cosh(p))$ )
- $I$  is the MEM image,  $M$  is a default image.
- MOSMEM options:
  - Initial image model and total FLUX constraint.
  - Joint deconvolution of a mosaic and single dish image.
  - Default image. e.g. can use single dish image as a default image.
- Best method depend strongly on the calibration and systematic errors.
  - convergence of MOSMEM depends on realistic RMS estimates.

- Gradient search algorithm:
  - primary beam weight the current MEM image
  - FFT to get predicted visibility  $V'$  from image and beam .
  - accumulate  $\chi^2$  over all pointings  $(x', y')$
  - generate new MEM image.
  - iterate until MEM image is consistent with the data.
- Maximum Entropy deconvolution pioneered by Tim Cornwell  
 find image which is consistent with all the data.  
 may be many such images, so chose the most likely one.  
 Maximum Entropy image subject to  $\chi^2$  constraints.  
 gradient search algorithm in MEM and  $\chi^2$  image.
- MIRIAD uses efficient user-friendly algorithm pioneered by Bob Sault.
- MOSMEM & MOSSDI look same as for single field deconvolution.
- Algorithms start with images and synthesized beams, not uv-data.







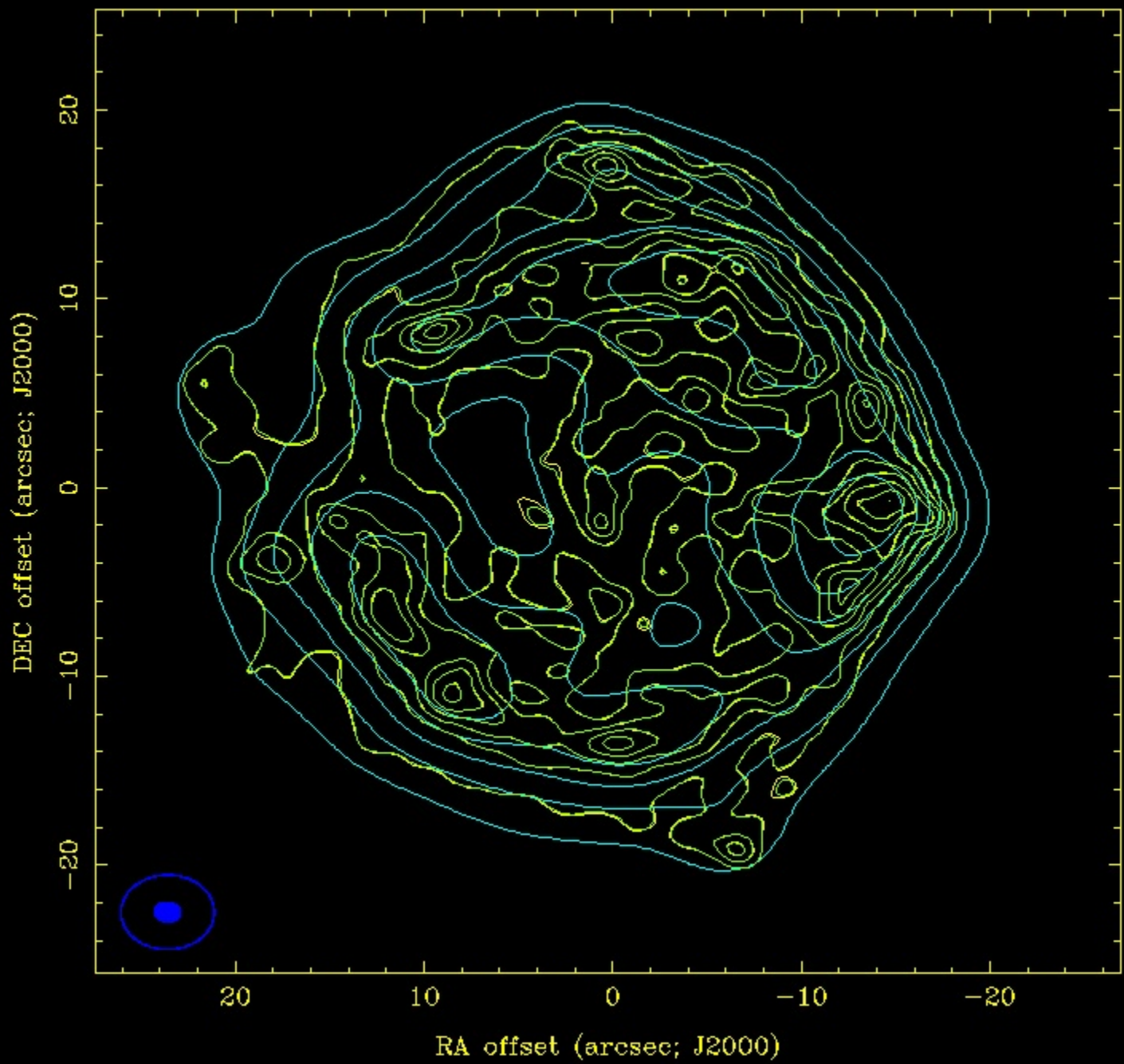


Figure 11: IMMERGE of ALMA and ACA, overlap in range 10-20  $k\lambda$

## 10 SAMPLING REQUIREMENT

- Nyquist sample interval for  $uv$  data,  $\delta uv = D_{ant}/2\lambda$ .
- Nyquist sample interval for pointings,  $\delta\theta = \lambda/2D_{ant}$ .
- Number of pointings,  $Npts \sim \Omega/(\delta\theta)^2$ .
- Nyquist sample rate  $\sim baseline/\lambda \times (2D_{ant}/\lambda)^2 \times 2\lambda/D_{ant} \times \Omega \times sdot$   
 $D_{ant}$  is antenna diameter,  $\Omega$ , source size, and  $sdot = 2\pi/24/3600$ .  
sample rate =  $\sim (1km/\lambda) \times 2\lambda/12m \times Npts \times 7.2710^{-5}$   
Nyquist sample rate  $\sim Npts/165$  per second.
- Same pointing pattern for 7 and 12m antennas.  
No loss in sensitivity; oversampled data are accounted for.
- Sample rate =  $baseline/\lambda \times 2\lambda/D_{ant} \times \Omega/(\lambda/2D_{ant})^2 \times sdot$   
larger antennas must sample faster.
- On-the-fly mosaicing is needed for imaging larger fields with ALMA.  
data rates are high to sample pointings and uv-data at Nyquist rate.

## 10.1 HEXAGONAL POINTING GRIDS

- Pointing grids must sample the source
- Custom grids easy to build using hexagonal patterns
- Hexagonal grid sampled at Nyquist spacing  $\lambda/2D_{ant}$ 
  - Oversampling by  $\sqrt{3}/2$  helps the mosaicing process
  - Less time per pointing, but no loss in sensitivity
- MIRIAD tasks: **hex**, **hexc**
- Mosaicing simulations in \$MIR/demo.

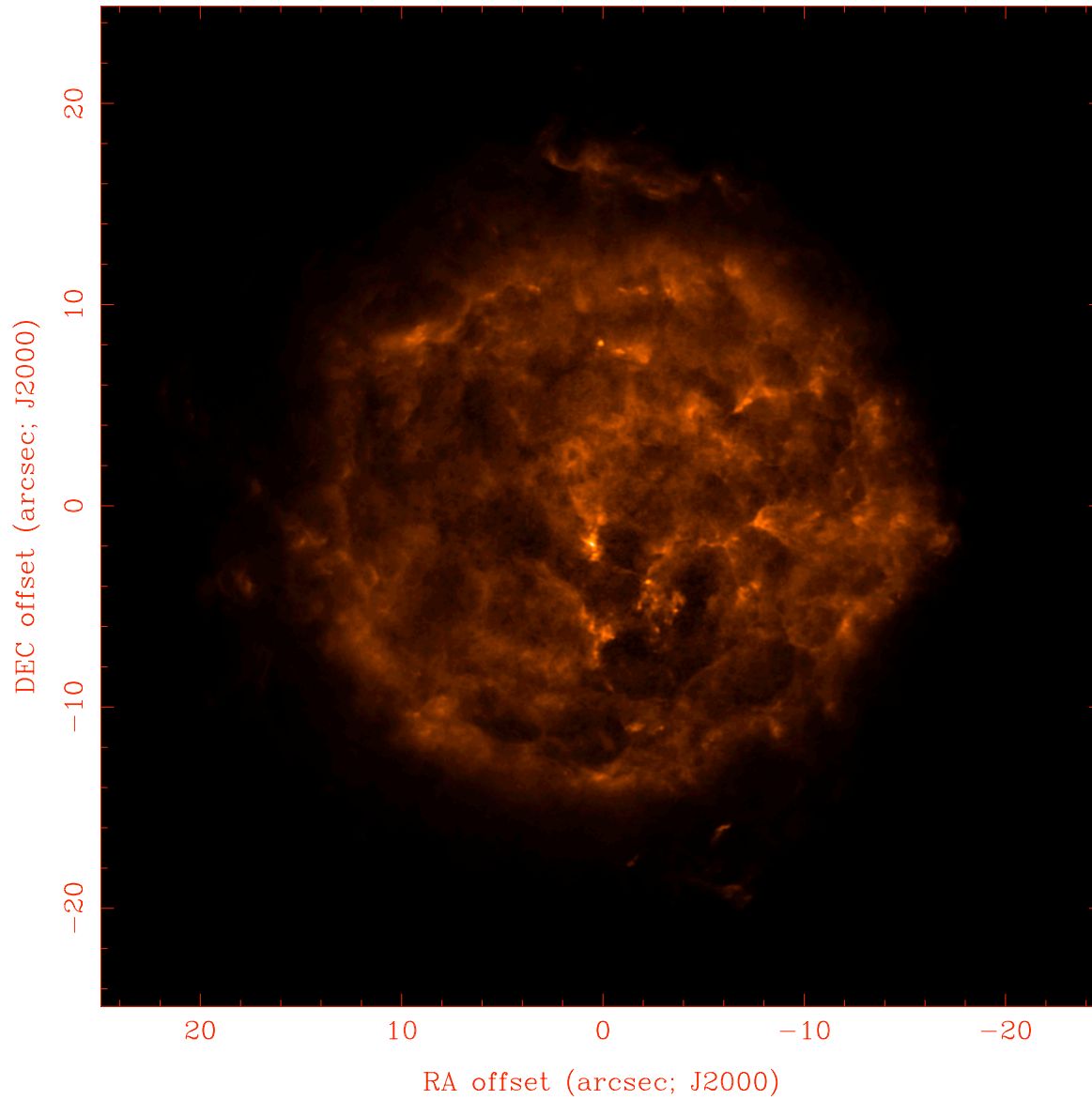


Figure 12: Scaled image of Cas A illuminated by ALMA 12 m antennas in a 19-pointing mosaic.

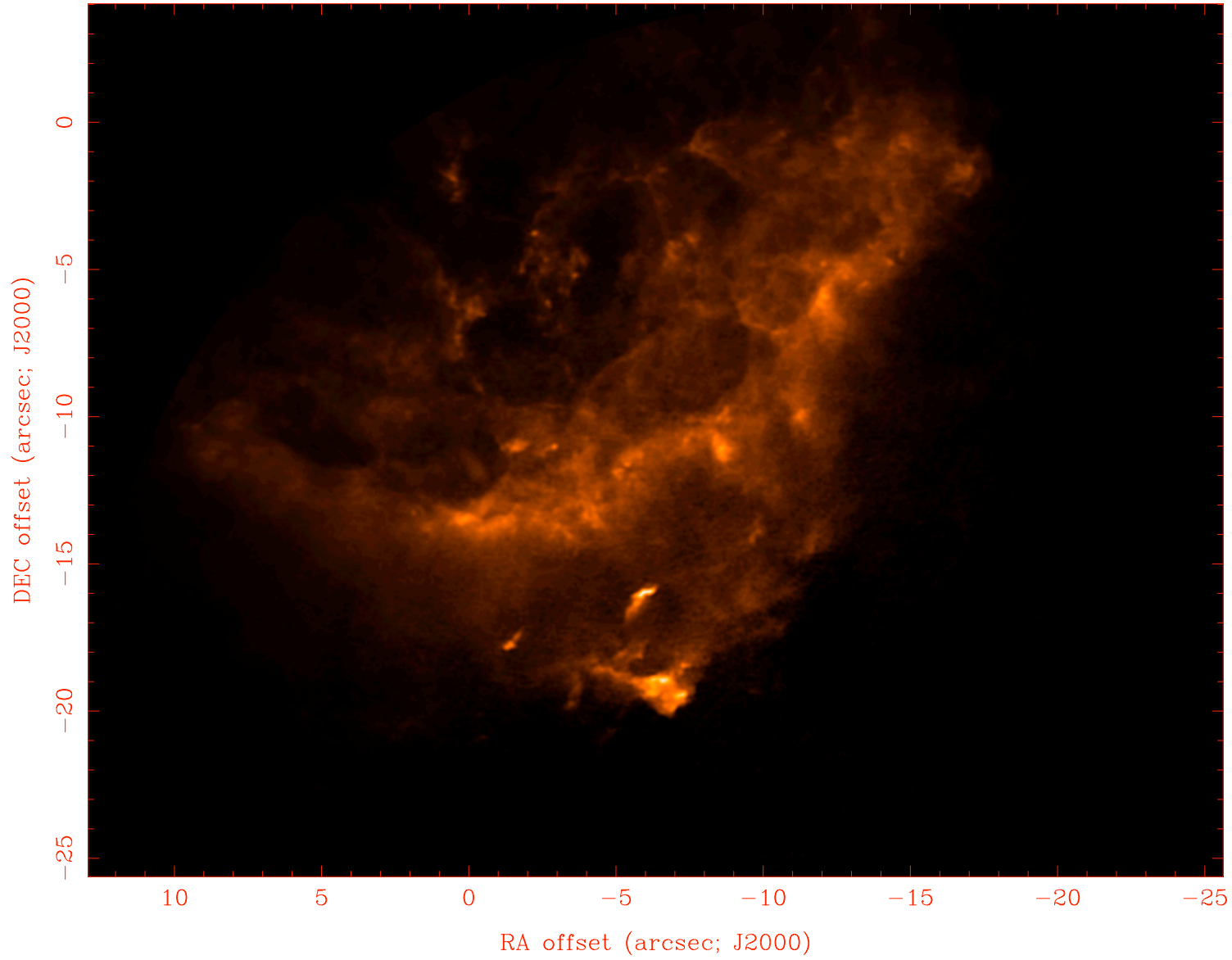


Figure 13: Scaled image of Cas A illuminated by ALMA 12 m antennas in a 19-pointing mosaic.

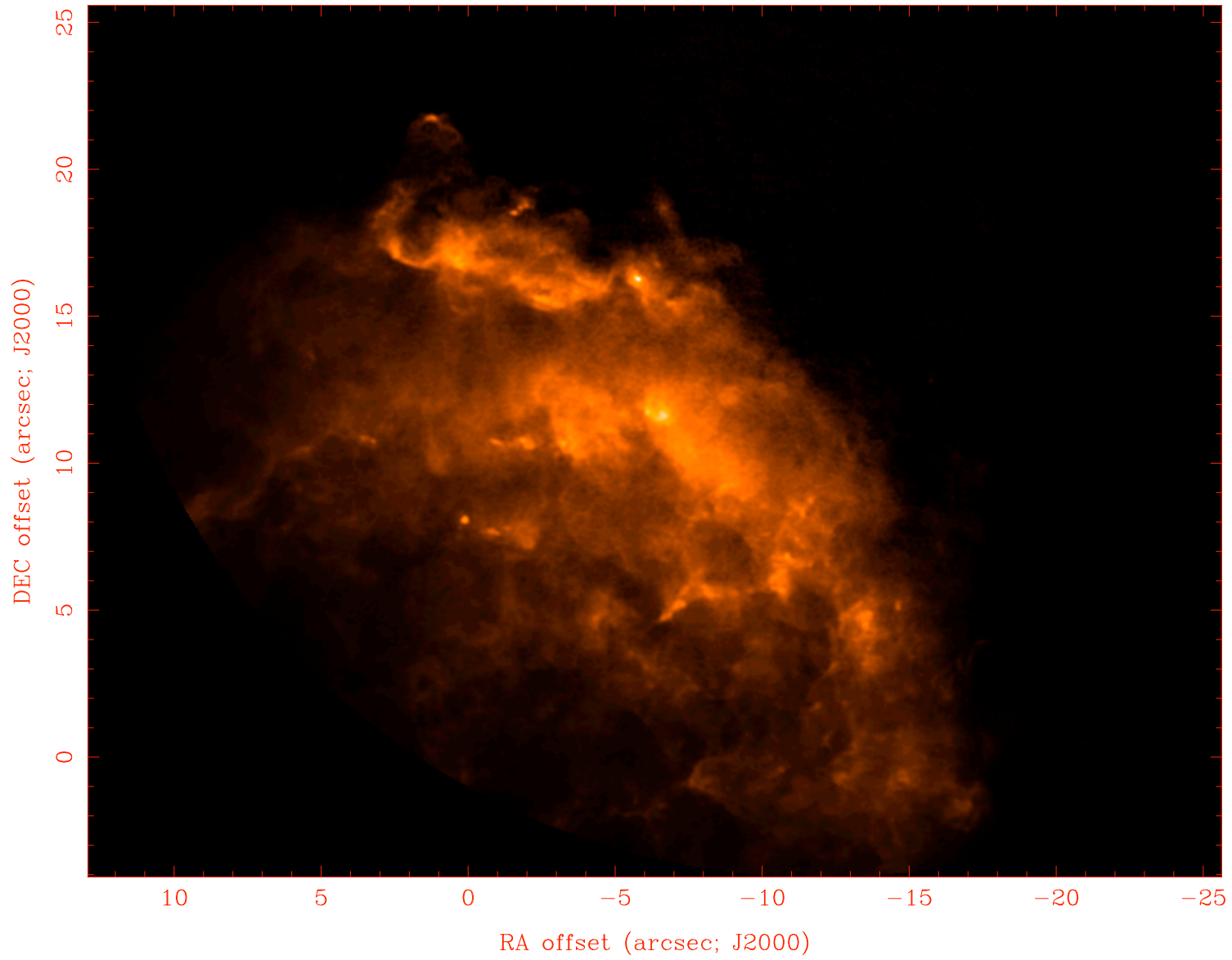


Figure 14: Scaled image of Cas A illuminated by ALMA 12 m antennas in a 19-pointing mosaic.

## 11 IMAGE FIDELITY AS A FUNCTION OF SOURCE SIZE

- ALMA can image  $\sim 24''$  diameter with 7-pointing mosaic at 230 GHz.  
 $\sim 32''$  diameter with a 19-pointing mosaic. (ALMA memo 430)
- Image fidelity decreases as the source size increases.
- Joint deconvolution gives the best image fidelity.
- Image fidelity very dependent on quality of single dish data.  
ACA can calibrate SD data for better low resolution image.
- Default image method is better for lower quality single dish data.
- Image fidelity improved by mosaic with ACA data.  
short spacings with 7m antennas sample large scale structure.  
cross calibrate single dish and interferometer observations.  
(ALMA memo 272 and memo 450)

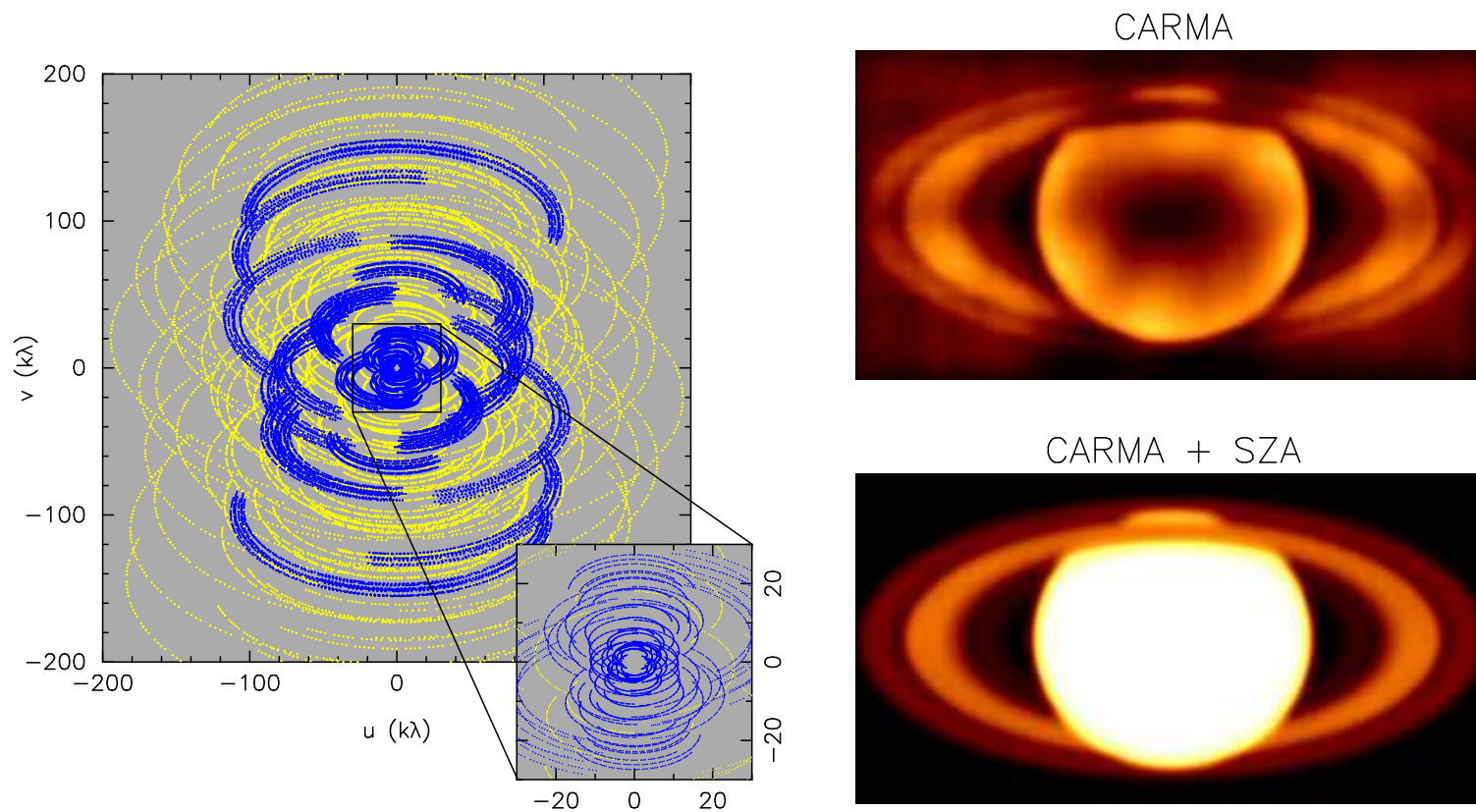


Figure 15: CARMA 23-element heterogeneous array. Left: uv data sampling at 100 GHz , DEC=30 . Yellow points: uv coverage for the CARMA 15-element array; blue points show the additional uv coverage when the 3.5-m antennas are used in the 23-element array. The dense uv sampling at short spacings shown in the inset, gives sensitivity to larger scale structure. Right: Simulated CARMA observations of Saturn show the increase in image fidelity for extended sources provided by the 3.5 m antennas.

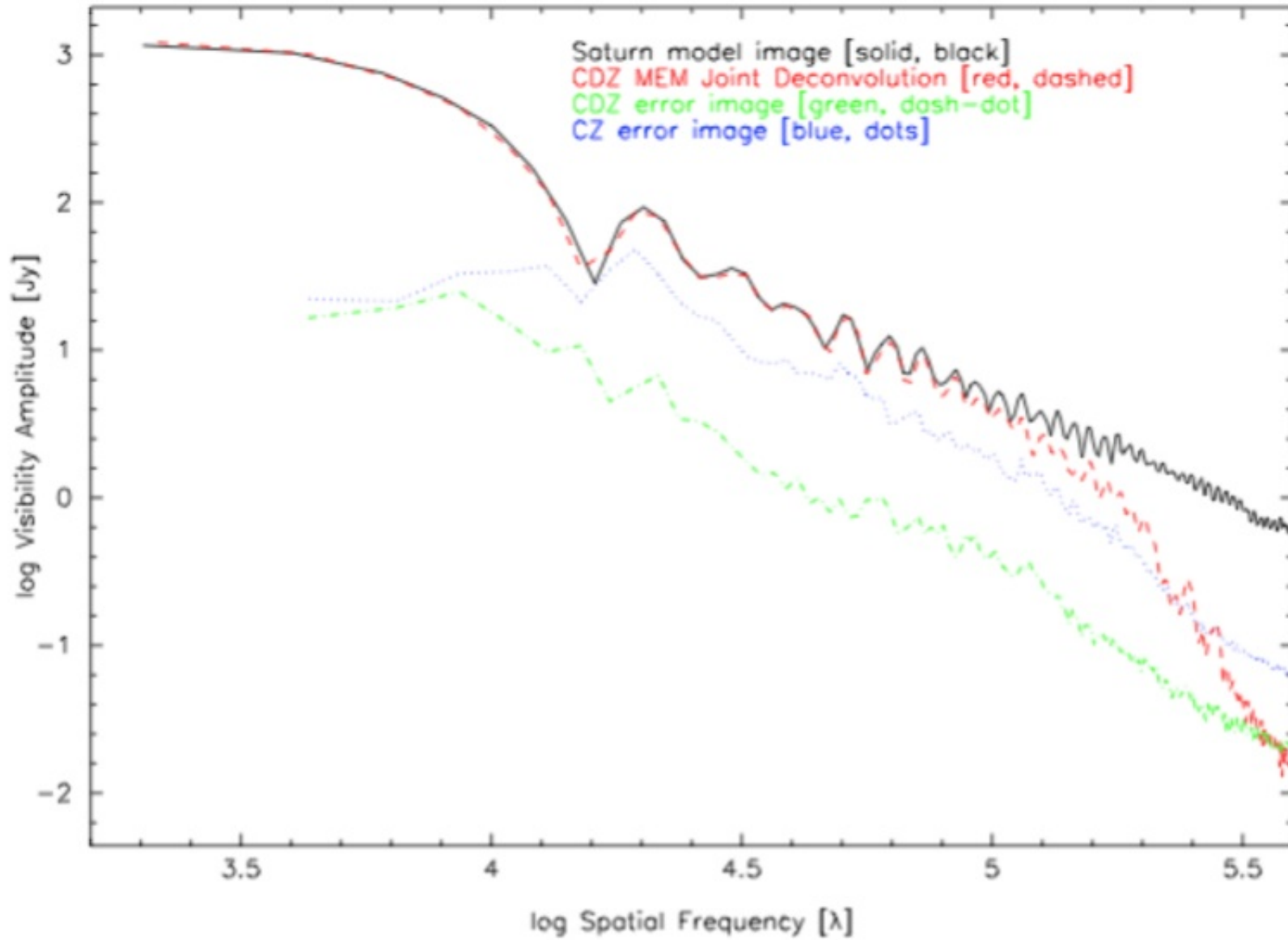


Figure 16: Simulated CARMA observations of Saturn show the image fidelity in the uv domain.

## 12 PRIMARY BEAMS IN MOSAICS

- **IMLIST options=mosaic** lists the mosaic table for an image.
- **MOSSEN** determines the RMS and GAIN of a mosaic image.  
Both are a functions of position and frequency dependent.
- **MOSPSPF** makes Point Spread Function for **invert options=mosaic**.
- **DEMOS** multiplies image by PB for multiple pointings.  
produces an image for each pointing center.  
this task performs the inverse of mosaicing.  
pointing centers and PBs are specified by the visibility dataset.  
output images, with PBs applied, are used to compare with uv-data
- **UVMODEL** processes uv-data using image model (add, subtract, multiply, divide, replace, flag).  
SELFCAL and UVMODEL handle multichannel uv-data with multiple pointings and PBs.

## 13 DECONVOLVING PRIMARY BEAM PATTERNS FROM MOSAICS

- Antennas measure the sky brightness weighted by primary beams.
- Usual assumption: PB is invariant, and the same for all antennas.  
Images of PB weighted sky brightness formed from FT of uv-data.  
sources larger than PB require a mosaic of interferometer  
and single dish observations at multiple pointing centers.
- If PB is time variable, and different on each antenna.  
deconvolve by subtracting model from uv-data (SKA memo 103).  
uv-data imaged using canonical, time invariant PB patterns.  
deconvolved using the measured PB voltage patterns.
- Existing software subtracts a model of the sky brightness from uv-data.  
subtract model of sky brightness weighted by measured PB patterns.  
residual uv-data re-imaged to provide an improved sky model.  
iterate until residual uv-data are consistent with noise.

## 14 CONCLUSION

- Simulations using scaled images of Cas A and Saturn as models.
- MIRIAD uses SD as uv-data, Default image, or Joint deconvolution.
- Best method depends on the nature of the errors in the data.
  - MOSMEM deconvolution mosaics using SD, ACA and ALMA.
  - Best image fidelity using Joint deconvolution of SD and ALMA data.
- The main source of errors are Primary Beam and pointing errors for ALMA at high frequency (ALMA memo 430, SKA memo 103)
- For larger mosaics, Image fidelity strongly depends on sources in FOV.
  - ”strong” sources must be calibrated and subtracted from uv-data.
  - Pointing and PB are best determined during observations.
  - Calibrations need to adapt to the sources detected in the FOV.
- Data rates are high to adequately sample large mosaics.

- EVLA and SKA problems are similar, but with more sources in the FOV, are more difficult.
- Data structure of CASA is poorly designed to handle these problems.
- Adaptive Real Time Imaging addresses these problems.
  - off-line data processing can not handle the data rate needed.
  - delayed calibration and analysis limit the science which can be done.
  - we must reduce the burden of data reduction.
  - provide real-time feedback to observers to optimize observations.

## References

- CARMA memo 38, 2007, *Image Fidelity as a Function of Source Size and Calibration Errors*, Melvyn Wright.
- CARMA memo 43, 2008, *Deconvolving Primary Beam Patterns from Mosaic and Polarization Images*, Melvyn Wright & Stuartt Corder.
- Cornwell, T.J., Holdaway, M.A. & Uson, J.M., 1993, *Radio-interferometric imaging of very large objects: implications for array design*, A&A 271, 697.
- Dunn, D.E., de Pater, I., Wright, M., Hogerheijde, M., and Molnar, L.A., 2005, *High Quality BIMA/OVRO Images of Saturn and its Rings at 1.3 and 3 mm*, AJ, 129,1109
- Ekers, R. D., & Rots, A.H. 1979, in IAU Col. 49, *Image Formation from Coherence Functions in Astronomy* , ed. van Schooneveld, C. (Dordrecht:Reidel), p.61
- Holdaway, M. A., 1998, *Mosaicing with Interferometer Arrays*, Synthe-

sis Imaging in Radio Astronomy II, ASP Conference Series, G. B. Taylor, C. L. Carilli and R. A. Perley (Eds)

Holdaway. M.A., 1999, *Mosaicing with Interferometer Arrays*, ASP Conference series 180, 401.

Nijboer, R. J., Noordam, J. E., 2005, *LOFAR Calibration*, Astronomical Data Analysis Software and Systems XVI ASP Conference Series, Vol. 376, 237, Richard A. Shaw, Frank Hill and David J. Bell. (Eds)

Nijboer, R. J., Noordam, J. E., Yatawatta, S. B., 2006, *LOFAR Self-Calibration using a Local Sky Model*, Astronomical Data Analysis Software and Systems XV ASP Conference Series, Vol. 351, 291, Carlos Gabriel, Christophe Arviset, Daniel Ponz, and Enrique Solano. (Eds)

Sault, R.J., Staveley-Smith, L & Brouw, W.N., 1996, *An approach to interferometric mosaicing*, A&A Supp. 120, 375

Sault, R.J., & Killeen, N., 2006, *Miriad Users Guide*, <http://www.atnf.csiro.au>

SKA memo 103, 2008, *Deconvolving Primary Beam Patterns from SKA Images*, Melvyn Wright & Stuartt Corder.

Wright, M.C.H., 1999, *Image Fidelity: Implications for ALMA*, ALMA memo 272.

Wright, M.C.H., 2002, *Compact Configuration Evaluation - Mosaicing*, ALMA memo 430.

Wright, M.C.H., 2003, *Heterogeneous Imaging with the ALMA Compact Array*, ALMA memo 450

Wright, M.C.H., 2012 *Adaptive Real Time Synthesis Telescopes*, The International Journal of High Performance Computing Applications Volume 26, No. 4.